Parkin Deficiency Suppresses Antigen Presentation to Promote Tumor Immune Evasion and Immunotherapy Resistance

Renzo Perales-Linares[1], Nektaria Maria Leli[1], Hesham Mohei[1], Silvia Beghi[1], Osvaldo D. Rivera[2], Nektarios Kostopoulos[1], Andrea Giglio[1], Subin S. George[3], Mireia Uribe-Herranz[1], Francesca Costabile[1], Stefano Pierini[1], Sergei Pustylnikov[1], Giorgos Skoufos[4], Yoseph Barash[2], Artemis G. Hatzigeorgiou[4], Constantinos Koumenis[1], Amit Maity[1], Michael T. Lotze[5,6,7], and Andrea Facciabene[1]

ABSTRACT

Parkin is an E3 ubiquitin ligase, which plays a key role in the development of Parkinson disease. Parkin defects also occur in numerous cancers, and a growing body of evidence indicates that Parkin functions as a tumor suppressor that impedes a number of cellular processes involved in tumorigenesis. Here, we generated murine and human models that closely mimic the advanced-stage tumors where Parkin deficiencies are found to provide deeper insights into the tumor suppressive functions of Parkin. Loss of Parkin expression led to aggressive tumor growth, which was associated with poor tumor antigen presentation and limited anti-tumor $CD8^+$ T-cell infiltration and activation. The effect of Parkin deficiency on tumor growth was lost following depletion of $CD8^+$ T cells. In line with previous findings, Parkin deficiency was linked with mitochondria-associated metabolic stress, PTEN degradation, and enhanced Akt activation. Increased Akt signaling led to dysregulation of antigen presentation, and treatment with the Akt inhibitor MK2206-2HCl restored antigen presentation in Parkin-deficient tumors. Analysis of data from patients with clear cell renal cell carcinoma indicated that Parkin expression was downregulated in tumors and that low expression correlated with reduced overall survival. Furthermore, low Parkin expression correlated with reduced patient response to immunotherapy. Overall, these results identify a role for Parkin deficiency in promoting tumor immune evasion that may explain the poor prognosis associated with loss of Parkin across multiple types of cancer.

Significance: Parkin prevents immune evasion by regulating tumor antigen processing and presentation through the PTEN/Akt network, which has important implications for immunotherapy treatments in patients with Parkin-deficient tumors.

Introduction

Adult tumors with secondary genomic instability escape from immune control, representing one of the primary challenges, affecting the design of cancer immunotherapies. Tumor editing by the immune system occurs with immune surveillance, resulting in the elimination of early-transformed cells. A subpopulation of immune-edited cancer cells can survive, entering equilibrium with the immune system, leading to a positive selection of poorly immunogenic cells that ultimately results in tumor growth, escape, and disease progression. One key mechanism of immune escape in cancer is the loss of antigenicity, which involves defects in the processing and presentation of tumor antigens including loss of MHC expression or dysregulation of antigen-processing machinery (1, 2).

Parkin, encoded by the *PRKN* gene, functions as an E3 ubiquitin ligase involved in the ubiquitination of several proteins and is critical in many cases in the development of Parkinson disease (PD). A growing body of epidemiologic, genetic, and biochemical evidence suggests that Parkin also functions as a tumor suppressor gene (3). For instance, the analysis of nonmalignant versus clear cell renal cell carcinoma (ccRCC) tissue samples confirmed that cancer tissues are associated with chromosomal losses of *PRKN*, and the downregulation of Parkin expression corresponds to high-grade ccRCC and lymph node (LN) metastasis, high tumor-specific mortality rates, and shorter overall survival (4). As Parkin defects are commonly carried by patients with PD, a large number of epidemiologic studies have reported that the occurrence of melanoma is higher than expected among subjects with PD, and the occurrence of PD is reciprocally higher than expected among patients with melanoma. Moreover, the study of *PRKN* in a cohort of 246 patients with melanoma showed that a mutation in Parkin-E28K impairs its ubiquitination and results in loss of its tumor suppressive activity (5). Parkin plays an important role in controlling cellular processes that can lead to cancer transformation, among other disorders. However, the mechanism by which Parkin deficiency in tumors shapes their antigenicity and immunogenicity remains elusive. Thus, investigating the role of Parkin in tumor antigen presentation is key to understanding tumor evasion.

The PI3K/Akt signaling network is central to regulation of cellular processes including proliferation, survival, motility, and immune modulation. Consequently, its dysregulation can result in cancer development (6). An important step in the success of cell-mediated antitumor

[1]Department of Radiation Oncology, University of Pennsylvania Perelman School of Medicine, Philadelphia, Pennsylvania. [2]Graduate Group in Cell and Molecular Biology, University of Pennsylvania, Philadelphia, Pennsylvania. [3]Penn Bioinformatics Core, University of Pennsylvania, Philadelphia, Pennsylvania. [4]Department of Computer Science and Biomedical Informatics, University of Thessaly - Hellenic Pasteur Institute, Athens, Greece. [5]Department of Surgery, University of Pittsburgh Medical Center Hillman Cancer Center, Pittsburgh, Pennsylvania. [6]Department of Immunology, University of Pittsburgh Medical Center Hillman Cancer Center, Pittsburgh, Pennsylvania. [7]Department of Bioengineering, University of Pittsburgh Medical Center Hillman Cancer Center, Pittsburgh, Pennsylvania.

Corresponding Author: Andrea Facciabene, Radiation Oncology, University of Pennsylvania, SCTR, Room 8-133, Philadelphia, PA 19104. E-mail: facciabe@pennmedicine.upenn.edu

Cancer Res 2023;83:3562–76

doi: 10.1158/0008-5472.CAN-22-2499

immunity is the processing and presentation of tumor-associated antigens. Recent studies have revealed that Parkin deficiency results in mitochondrial stress, the degradation of the tumor suppressor PTEN (natural inhibitor of PI3K) through S-nitrosylation, and enhanced PI3K/Akt activation (7, 8). Importantly, the loss of PTEN attenuates the induction of MHC-I, MHC-II, and STAT1 by IFNγ stimulation. Over activation of Akt can repress these signals (9). There might therefore be an unexplored link between Parkin and tumor evasion through the PI3K/Akt signaling pathway.

Parkin has been directly connected to MHC-I antigen presentation in the context of PD. A recent study characterized a mitochondrial antigen presentation (MitAP) pathway suppressed by PINK1 and Parkin, which through a network of mitochondrial-derived vesicles (MDV), facilitates mitochondria self-antigen presentation on MHC-I (10). Once at the cell surface, the mitochondria-derived antigens are capable of triggering an immune response. Because PINK1 and Parkin oversee mitochondria quality control and are present with the associated genetic and functional defects in PD, the poor control over MitAP implicates a new mechanism to explain neurodegeneration through autoimmunity in patients with PD. We previously demonstrated that tumor-associated mitochondrial antigens (TAMA) can be utilized in a dendritic cell (DC)–based immunization strategy (prophylactically and therapeutically) to control tumor growth in a murine model of renal cell carcinoma (11). Accordingly, based on the MitAP model, we hypothesized that genetically removing Parkin from tumors would affect the efficiency of the vaccine and increase tumor antigenicity. Surprisingly, however, we found quite a different outcome.

In this study, we show that the tumor-intrinsic loss of Parkin disrupts antigen processing and presentation through the dysregulation of the PTEN/PI3K/Akt signaling cascade. Moreover, the loss of or defects present in Parkin through the progression of cancer define the antitumor $CD8^+$ T-cell reactivity, facilitating tumor evasion.

Materials and Methods

Animals and cells

Six- to 8-week-old BALB/c (H-2d), C57BL/6 (H-2b), and OT1 [strain C57BL/6-g(TcraTcrb)1100Mjb/J)] mice were purchased from The Jackson Laboratory. The murine renal carcinoma RENCA (H-2d) and the melanoma B16-F10 engineered to express ovalbumin (B16-OVA; H-2b) cell lines were purchased from the ATCC. G418 (500 μg/mL) was used for positive selection of B16-OVA–transfected cells. Similarly, the HEK293 and human ccRCC lines (A498, 786-O, CAKI-1) were provided by the same vendor. Cells were propagated in 5% CO_2 at 37°C and cultured in RPMI1640 medium with 2 mmol/L L-glutamine and 25 nmol/L HEPES (Corning) or DMEM with 4.5 g/L glucose, L-glutamine and sodium pyruvate (Corning), were supplemented with 10% FBS (GIBCO), 1 mmol/L sodium pyruvate (GIBCO), 2 mmol/L nonessential amino acids (GIBCO), 100 U/mL penicillin, and 100 mg/mL streptomycin (Corning). Cells were discarded by passage 12. All cells were tested for *Mycoplasma* contamination before expansion, aliquot, and cryopreservation.

Plasmids and lentiviruses

The lentivirus packaging plasmids psPAX2 (catalog no. 12260) and pCAG-VSVG (catalog no. 64084) as well as the GeCKO_V2 backbone (catalog no. 52961), in which individual sgRNAs were cloned, were purchased by Addgene. The mouse homolog for Parkin overexpression was designed to express a wild-type Prkn, which is not recognized by Cas9 and was purchased by Vector Builder (#VB190910–1157aev).

Lentivirus was made in HEK 293T cells by cotransfecting lentiviral vector and packaging plasmids with lipofectamine 2000 (11668019; Thermo Fisher Scientific) according to the manufacturer's instructions. The virus-enriched supernatant was collected 48 to 72 hours posttransfections. Supernatant was centrifuged at 2,000 × *g* at 4°C for 10 minutes and then the supernatant was passed through a 0.45 μm filter (Millex-HV, SLHV033PS).

Generation of stable cell lines

For the generation of stable Parkin-deficient knockdown RENCA cells, lentivirus was generated with shRNA Prkn (TRCN0000041143, sh#1; TRCN0000041145, sh#3), or empty vector in the pLKO.1 Puro backbone (Addgene, 8453). For the generation of the CRISPR knockout cell lines, sequences targeting human and mouse Prkn were designed and cloned within the GeCKO-V2 lentiviral vector as described previously (12). A GeCKO-V2 empty vector plasmid that did not undergo CRISPR–Cas9-mediated gene editing was used as empty vector control. The primers used for the introduction of the sgRNA into the GeCKO_V2 backbone are hU6-F (5′-GAGGGCCTATTTCCCATGATT-3′) or pLKO.1 (5′-GACTATCATATGCTTACCGT-3′). The targeting sites for human *PRKN* were GTGTCAGAATCGACCTCCAC (exon 1) and GCATTACGTGCACAGACGTC (exon 4), and for mouse *Prkn* GTGTCAGAATCGACCTCCAC (exon 1; same as human) and AGGGCCCATCTTGC (exon 4). The sequence of the vector overexpressing wild-type *PRKN* was designed to have silent mutations around the sgRNA recognizing areas. The sequences above were replaced with GTCGAAGTTGACTCAGATACC (exon 1) and CAAGG TCCGTCCTGT (exon 4). Infected Parkin-deficient (shRNA or CRISPR/Cas9) and Parkin-overexpressing cells were selected in the presence of 1 μg/mL puromycin (InvivoGen, ant-pr-5b) or 1 μg/mL blasticidin (InvivoGen, ant-bl-1), respectively, for 2 weeks. Isolation of *PRKN* clonal deletion mutants was validated by immunoblotting and RT-PCR analysis. All cells were tested to discard mycoplasma contamination.

Tumor challenge

Six- to 8-week-old mice were injected subcutaneously in the back with 1×10^6 RENCA or B16-OVA cells per mouse. Solid tumor development was monitored by caliper measurements every other day from the day they were palpable. Experiments were terminated when Parkin-deficient mouse tumors reached 2 cm^3 (according to the University of Pennsylvania guidelines). The orthotopic tumor challenge was performed following the methods of Ishihara and colleagues (13). Briefly, 1×10^6 Parkin-deficient or empty vector control RENCA cells were injected into the kidney capsule of 4 mice per group and monitored tumor growth for 14 days

In vivo CD8 blocking treatment

Mice received via intraperitoneal injections of 1 mg/mL of monoclonal blocking antibody (200 μL; InVivoMAb antimouse CD8a; clone YTS 169.4. BioXCell) or isotype control (InVivoMAb rat IgG2b isotype control; clone LTF-2. BioXCell), 2 days prior tumor, on the day of tumor injection, and then, 2 times per week/every 4 days.

TAMAs vaccine and *ex vivo* DC preparation

As described previously (11), mitochondria were purified from RENCA cell lines using a discontinuous sucrose gradient. Preparations were frozen (liquid nitrogen) and thawed (37°C, water bath) for three cycles, sonicated, and irradiated at 5,000 rad for sterilization. Quantification was carried out with the BCA assay. BALB/c-derived bone marrow cells were harvested from the mouse femur, seeded in 6-well

plates and incubated with GM-CSF and IL4 at concentrations of 10 ng/mL for 7 days. Media was refreshed every 2 days. On day 7, DC were collected and adjusted to 1×10^6 cells/mL and incubated with 1 μg/mL LPS (Invivogen, tlrl-eblps), 0.1 μg/mL IFNγ (Peprotech, 315–05), and pulsed with mitochondria lysate (50 μg/mL), overnight. Mice were injected subcutaneously 3 days after tumor challenge with 0.5×10^6 mitochondria-pulsed DC, and then given two more injections at weekly intervals.

RT-PCR

The relative quantification of the expression levels of selected genes was carried out by qPCR. Total RNA from cells and tissues was extracted using TRIzol reagent (Invitrogen, 15596018) according to the manufacturer's instructions. Reverse transcription and RT-PCR reactions were carried out using the High Capacity cDNA Reverse Transcription Kit (Thermo Fisher Scientific, 4368814) and TaqMan Gene Expression Master Mix (Thermo Fisher Scientific, 4369016) according to the manufacturer's instructions. Runs were performed using the QuantStudio 6 Flex Real-Time PCR System (Thermo Fisher Scientific). All TaqMan primers were purchased from Thermo Fisher Scientific. Housekeeping gene *Rn18s* (Mm03928990_g1), *PRKN* (Hs01038322_m1), *Prkn* (Mm01323528_m1), *H2-k1* (Mm01612247_mH), *Tap1* (Mm00443188_m1), *Psmb8* (Mm00440207_m1), *B2m* (Mm00437762_m1), *Ifng* (Mm01168134_m1), *Ifnb* (Mm00439552_s1), *Foxp3* (Mm00475162_m1), *Il12b* (Mm01288989_m1), and *Gzmb* (Mm00442837_m1).

Immunoblotting

Whole-cell protein lysates were processed using RIPA buffer, supplemented freshly with a protease and phosphatase inhibitor cocktail (Thermo Fisher Scientific, 1861231) and EDTA (5 mmol/L), following the manufacturer's instructions. SDS-PAGE was performed using the Bio-Rad Mini-protean TGX (4%–20%) gels and after electrophoresis, protein transfer was done using the Trans-Blot Turbo Transfer System. Chemiluminescence signals were detected on the Chemi-Doc MP (Bio-Rad). The primary antibodies for TAP1, PSMB8, β2-microglobulin (D8P1H), HSP90 (C45G5), β-actin (E4D9Z), Vinculin (VCL; E1E9V), Parkin, PTEN, AMPKa, phospho-AMPKa (Thr172; 40H9), Akt, phospho-Akt (Ser473; D9E), phospho-GSK-3β (Ser9, D85E12), and GSK-3β (D5C5Z) were purchased from Cell Signaling Technology; HLA-A was purchased from Thermo Fisher Scientific; and MHC-I (ER-HR52) was obtained from Santa Cruz Biotechnology. All quantifications (Supplementary Figs. S6A–S6E) are done with every protein's respective housekeeping blot, except for the phosphorylated ones, which are normalized to their total protein or both, or unless specified otherwise

Flow cytometry

Cells were subjected to flow cytometry on a FACS Canto flow cytometer using BD FACS Diva software (BD Biosciences) and data were analyzed using FlowJo version X (TreeStar). The following mAbs against mouse markers were used to phenotype the T cells: anti-CD45 (clone 30-F11, Invitrogen) anti-CD3 (clone 17A2, BD Pharmingen), anti-CD4 (clone RM4–5, BL), and anti-CD8 (clone 53–6.7, BioLegend). iTAg Tetramer/PE–H-2 Kb OVA (SIINFEKL; MBL International) was used to detect specifically infiltrating OVA T cells. LIVE/DEAD Fixable Aqua Dead Cell Stain (Life Technologies) was used to gate living cells. The mAbs anti-Parkin (PRK8, Abcam), anti-MHC-I (H-2Kd; SF1–1.1.1, eBioscience), and anti–H-2kb bound to SIINFEKL (clone 25-D1.16, BL) were used to characterize the RENCA and B16-OVA cell lines.

ELISpot for IFNγ

We followed the ELISpot protocol as described elsewhere (14). Briefly, tumor cells were prestimulated with various reagents according to the experimental setting for 24 hours and then, cells were washed with PBS prior plate seeding. Upon plate preparation, RENCA or B16-OVA cells (1×10^4 cells/well) were cocultured for 16 hours in triplicates with T cells from TAMA-vaccinated or OT.1 mice (5×10^4 cells/well), respectively. After incubation, plates were washed with PBS and Tween 20, ELISPOT was performed, and spots were counted using an automated ELISPOT reader (Autoimmun Diagnostika).

Synthetic peptides

Splenocytes were stimulated for 16 hours with the 100 ng/well of the following peptides: mutated COX1291–306 (MFTVGLDVDTRTYFT), COX1295–310 (GLDVDTRTYFTSATM), and COX1299–314 (DTRTYFTSATMIIAI; Eunoia Biotech); and mutated ND5516–535 (SFSTLLGFFTSIIHR), ND5520–539 (LLGFFTSIIHRITPM), and ND5524–543 (FTSIIHRITPMKSLN; Mimotopes; ref. 11). After seeding in triplicates and incubation, ELISPOT was performed and spots were counted using an automated ELISPOT reader (Autoimmun Diagnostika).

ELISA

A498 cells were prestimulated for 24 hours with various experimental conditions and then, cells were washed with PBS. Next, tumor cells were cocultured with NY-ESO-1 T cells (donor 401; Astarte Biologics, 1093) for 16 hours. The next day, supernatants were collected and cleared by centrifugation. The levels of IFNγ were evaluated using the Human IFNγ DuoSet ELISA Kit (R&D Systems, DY285B) and following the manufacturer's instructions.

MTT assay

A total of 5,000 cells/well were seeded into a 96-well plate and cultured for overnight at 37°C in an incubator with 5% CO_2. After 24, 48, and 72 hours, 15 μL (5 mg/mL) MTT was added to each well for 4 hours, after which, the supernatants were removed carefully. Next, the MTT formazan was dissolved in 150 μL DMSO and optical density (OD) values were measured using a microplate reader at 492 nm. All assays were repeated three times.

ATP levels and nitric oxide synthase activity measurements

ATP levels and nitric oxide synthase activity were evaluated by the ATP Assay Kit from Abcam (catalog no. ab83355) and the Nitric Oxide Synthase Activity Assay Kit from Biovision (catalog no. K205–100) following the manufacturer's instructions, respectively. Briefly, Parkin-deficient or control cells were seeded in a 96-well plate and incubated in 2%-FBS cell culture medium at 37°C and 5% CO_2 for 18 hours. Absorbance was determined with a microplate reader at OD 570 nm (ATP levels) or OD 540 nm (nitric oxide synthase activity).

Whole-genome RNA sequencing and analysis

Total RNA from tumor tissues was extracted using TRizol reagent (Invitrogen, 15596018) according to the manufacturer's instructions. The sample quality had the following characteristics: RNA integrity number >6.0, ≥50 ng/μL, A260/A280 = 1.8–2.2, DNA free. RNA degradation and contamination was monitored on 1% agarose gels. RNA purity was checked using the NanoPhotometer spectrophotometer (IMPLEN). RNA integrity and quantitation were assessed using the RNA Nano 6000 Assay Kit of the Bioanalyzer 2100 system (Agilent Technologies). The RNA sequencing data set and libraries were prepared and sequenced at Novogene Corporation Inc. Briefly, the messenger RNA was purified from total RNA using poly-T oligo-

attached magnetic beads. After fragmentation, the first-strand cDNA was synthesized using random hexamer primers, followed by the second-strand cDNA synthesis using either dUTP for directional library or dTTP for nondirectional library. Quantified libraries were pooled and sequenced on the Illumina HiSeq platform. The raw reads were processed by removing the adaptor reads and low-quality tags. Clean reads for each sample were mapped to GRCm38/mm10 using the software HISAT2 (v2.0.5). featureCounts v1.5.0-p3 was used to count the reads numbers mapped to each gene. Then, FPKM of each gene was calculated on the basis of the length of the gene and reads count mapped to this gene. The differential expression analysis was performed using the DESeq2R package (v1.20.0). The *P* values were adjusted using the Benjamini and Hochberg method. Genes with an adjusted *P* value ≤0.05 found by DESeq2 were assigned as differentially expressed. The FASTQ raw data files are not available as they were inadvertently misplaced. However, the summary of gene expression data of the individual tumors included in this study is available as a supplemental file (Supplementary Table S1).

The Cancer Genome Atlas data acquisition

For **Fig. 4**, gene expression values represent FPKM normalized reads from publicly available deidentified patient data downloaded from the Clear Cell Renal Cell Carcinoma Project of The Cancer Genome Atlas [TCGA-kidney renal clear cell carcinoma (KIRC)]. Hg38 reference genome data were used and FPKM values for PRKN gene expression were calculated as described previously in the HTSEQ-FPKM pipeline issued by the GDC. Data were downloaded and harmonized using TCGAbiolinks (http://doi.org/10.1093/nar/gkv1507). Array-Array Intensity correlation (AAIC) was used to define a square symmetric matrix of Pearson correlation among samples to find and remove those samples with extremely low correlation (less than 20% correlation), which could be identified as possible outliers across the patient cohort. Clinical and Biological Specimen Databases for TCGA-KIRC project were also downloaded using TCGABiolinks. Clinical Database was used to calculate survivability. Biological Specimen Database was used to find matched normal tissue samples. Paired Student *t* test was used to compare differences in mean PRKN gene expression levels between normal and tumor tissue across the 72 matched patient samples found within the TCGA-KIRC dataset. Classification bins (low, mid, high) for PRKN gene expression levels (FPKM) were generated by using the entire population of 538 patients with KIRC and calculating three quantiles each representing 33% of the data. Kaplan–Meier estimators were used to plot survival probabilities across patient bins. Overall log-rank test was used to calculate the significance of trend between (low, mid, high) *PRKN* gene expression levels and survival probability. Two-group log-rank test was used to determine significant differences in patient survival between "low" and "high" *PRKN* gene expression bins across KIRC tumor stages I, II, II, and IV.

Supplementary Fig. S5 was produced using TCGA gene expression profiles from the KIRC cohort. For each patient with KIRC, RSEM-normalized gene expression counts were retrieved from the Broad GDAC Firehose browser (http://firebrowse.org/?cohort=KIRC&download_dialog=true). Subsequently, immunotherapy-treated patients were divided into two groups according to *PRKN* expression: low *PRKN* expression (below first quartile) and high *PRKN* expression (above third quartile). Survival analysis using Kaplan–Meier and the log-rank test between *PRKN*-low and *PRKN*-high groups was performed using the R package survival. Kaplan–Meier plots were produced using R package ggplot.

Statistical analysis

Sample sizes were chosen on the basis of pilot experiments and on our experience with similar experiments. Two-tailed Student *t* tests and two-way ANOVA were used to compare data sets where indicated. Survival over time was analyzed using the Kaplan–Meier estimator. A *P* value less than 0.05 was considered significant. Correction for FDR was used to correct for multiple comparisons. The heatmap was generated using the package Pheatmap (version 1.0.12) within the statistical and graphical software, RStudio (version 1.3.1093). Kyoto Encyclopedia of Genes and Genomes (KEGG) Enrichment Scatter Plot; rows show enriched terms, and the *y*-axis shows GeneRatio—which is the ratio between the number of differentially expressed genes in each enriched term and all the differentially expressed genes found in the KEGG database. The size of each dot represents the number of genes that are differentially expressed within each enriched term, and the color represents the adjusted *P* value for each enriched term. KEGG Enrichment Histogram shows the significantly enriched terms ($P_{adj} < 0.05$) in the KEGG enrichment analysis between groups, where the *x*-axis shows log of the adjusted *P* value ($-\log10[P_{adj}]$) and the *y*-axis shows the top 20 significantly enriched terms and the number of differentially expressed genes in each pathway, shown as *n*.

Study approval

All animal studies were approved by the Institutional Animal Care and Use Committee and the University Laboratory Animal Resources at the University of Pennsylvania. Mice were treated in accordance with University of Pennsylvania guidelines.

Data availability

The TCGA-KIRC gene expression profiles and de-identified patient clinical data analyzed in this study can be obtained without special access using the TCGAbiolinks software (https://bioconductor.org/packages/release/bioc/html/TCGAbiolinks.html) and the Broad GDAC Firehose portal (http://firebrowse.org/?cohort=KIRC&download_dialog=true). The RNA sequencing FASTQ raw data files were misplaced, but the summary gene expression data (Supplementary Table S1) of the individual tumors included in this study is available as a Supplementary File. All other raw data are available upon request from the corresponding author.

Results

Parkin regulates the MHC-I-associated tumor antigen presentation machinery and fosters tumor progression

To investigate the role of Parkin in association with expression of the MHC class-I antigen presentation machinery (APM) in tumors, we generated stable *Prkn*-deficient murine renal cell carcinoma (RENCA) cells using lentiviral shRNA (**Fig. 1A** and **C**). Because antigen presentation to $CD8^+$ T lymphocytes only occurs in the context of MHC-I expression, we characterized the APM associated with this pathway. We observed a positive association between Parkin-deficient cells and significantly reduced mRNA (**Fig. 1B**) and protein (**Fig. 1C**) expression levels of APM molecules MHC-I (*H2-k1*), *Tap1, Psmb8,* and *B2m*. Next, we tested the antigen presentation capabilities of the knockdowns in a coculture setting with T cells from TAMA-vaccinated mice. Consequently, deficiency in Parkin resulted in poor antigen presentation and T-cell activation (**Fig. 1D**). To evaluate the impact of Parkin-deficiency in tumor development, we challenged Balb/c mice with 1×10^6 *Prkn* knockdown (sh#1–3) or empty-vector (pLKO.1) control cells subcutaneously or orthotopically (intra-kidney) and monitored for tumor growth. In both models, Parkin-deficient tumors grew significantly faster than pLKO.1 controls (**Fig. 1E**;

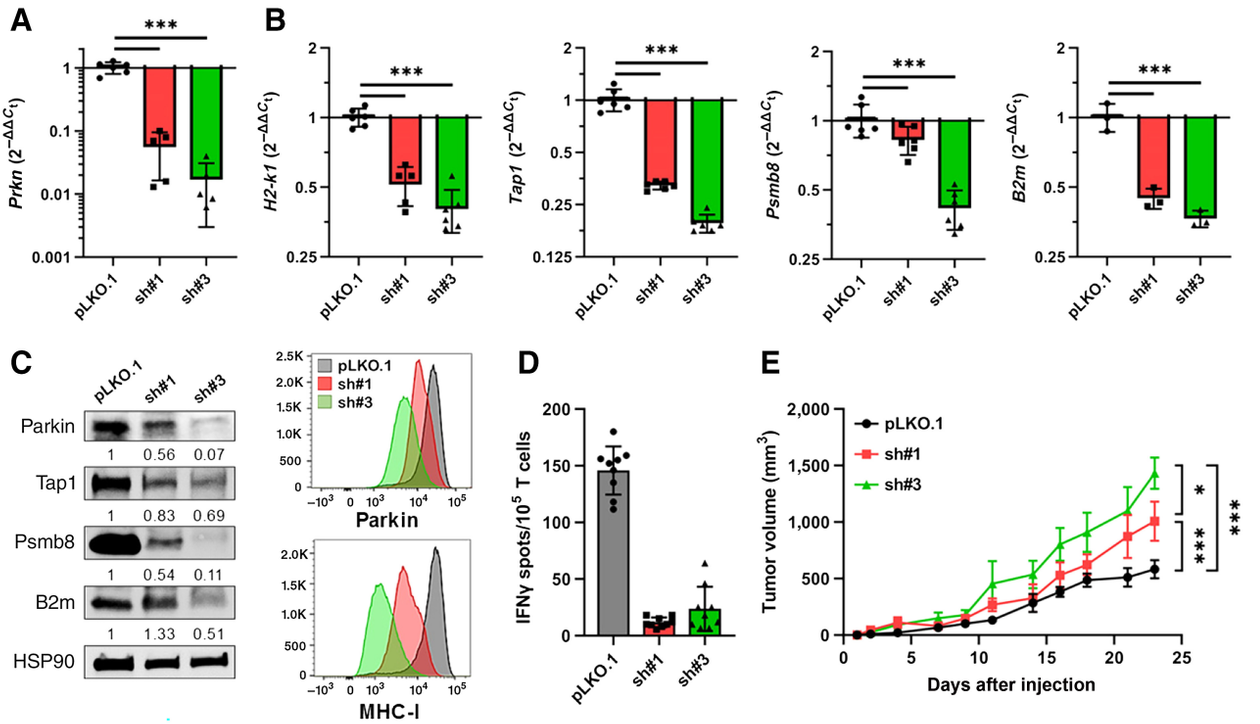

Figure 1.

Parkin regulates the MHC-I-associated tumor APM and fosters tumor progression. **A** and **B,** mRNA expression levels of *Prkn*, *H2-k1*, *Tap1*, *Psmb8*, and *B2m* in RENCA cells stably transfected with sh*Prkn*_1 (sh#1), sh*Prkn*_3 (sh#3), and empty vector control (pLKO.1) lentiviral vectors. Data are represented as mean ± SD. ***, $P < 0.001$; unpaired, two-tailed *t* test. **C,** Protein expression analyses of Parkin, Tap1, Psmb8, and B2m (immunoblotting) and Parkin vs. MHC-I (intracellular staining, flow cytometry) of pLKO.1 controls, sh#1, and sh#3 RENCA cells. Data represent two to three independent experiments. **D,** IFNγ ELISPOT analysis was performed on T cells isolated from the spleens of pLKO.1 RENCA tumor-bearing mice at day 25 after challenge. T cells were cocultured overnight with stimulator Parkin-positive (pLKO.1) or -negative (sh#1, sh#3) RENCA cells (5:1 ratio). **E,** Parkin-positive (pLKO.1) or -negative (sh#1, sh#3) RENCA cells (10^6) were injected in the back of BALB/c mice and tumor growth was monitored. Data are represented as mean ± SEM. *, $P < 0.05$; ***, $P < 0.001$; two-way ANOVA.

Supplementary Figs. S1A–S1D). Importantly, the most aggressive phenotype corresponds to the RENCA sh#3 tumors, also associated with the lowest Parkin and MHC-I expression levels. Subsequent experiments used the RENCA sh#3 cell (KD) because its phenotype significantly differs from control. Altogether, our data suggest that Parkin determines the APM expression levels in RENCA cells, with its depletion resulting in poor tumor antigen presentation in the context of MHC-I, consequently facilitating tumor growth. Because of the comparable outcomes observed in both the subcutaneous and orthotopic models, we opted to proceed with the subcutaneous model for our experimental plan, as it provides greater convenience and flexibility in terms of maneuverability.

Lack of Parkin undermines the effectiveness of a tumor-associated mitochondria antigen DC immunization

The Pink1/Parkin axis can regulate mitochondria-derived antigen presentation in RAW macrophages (10); however, the extent of its role in the context of tumor immunology is still not clear. To confirm the impact of Parkin-deficiency over mitochondria-derived antigen presentation in the RENCA tumor model, we utilized our previously reported TAMA DC immunization strategy employing mitochondria extracts (11) to prime and expand RENCA mitochondria-specific TCR. This immunization relies on the presence of mitochondria antigens derived from the cytochrome oxidase 1 (COX1) and the β-nicotinamide adenine dinucleotide, reduced (NADH) subunit 5 (ND5) mutations uniquely present in RENCA cells. Following tumor challenge, the DC-TAMA vaccine was injected subcutaneously once per week for 3 weeks and tumor growth was monitored until tissue collection (day 20). Similar to our previous observations, KD (sh#3) tumors grew significantly faster and larger than pLKO.1 controls. Notably, although the DC-TAMA vaccine effectively controlled tumor growth in the pLKO.1 group, it became ineffective in mice bearing tumors lacking Parkin (**Fig. 2A**). We investigated lymphocyte populations in tumors, draining lymph nodes (dLN), and spleen. We found a significant increase of $CD8^+$ T cells infiltrating pLKO.1/$TAMA^+$ tumors when compared with pLKO.1/$TAMA^-$ controls. However, this difference was not found in Parkin-deficient tumors (**Fig. 2B**). Of note, $CD45^+$ and $CD4^+$ T-cell subpopulations were not affected by the absence of Parkin in tumors (Supplementary Figs. S2A–S2C). Interestingly, we found significantly reduced $CD8^+$ T cells in KD dLN, either vaccinated or not, when compared with the pLKO.1 groups (**Fig. 2C**) and no differences of this cell population in the spleens across the studied groups (**Fig. 2D**).

To confirm that mice bearing KD tumors were positively vaccinated, magnetically isolated T cells were costimulated overnight with a cocktail of COX1/ND5 peptides. The next day, IFNγ-producing T cells were quantified by ELISpot analysis. TAMA-vaccinated mice bearing Parkin-deficient tumors presented a significant reduction of T-cell activation upon peptide stimulation as compared with their TAMA-

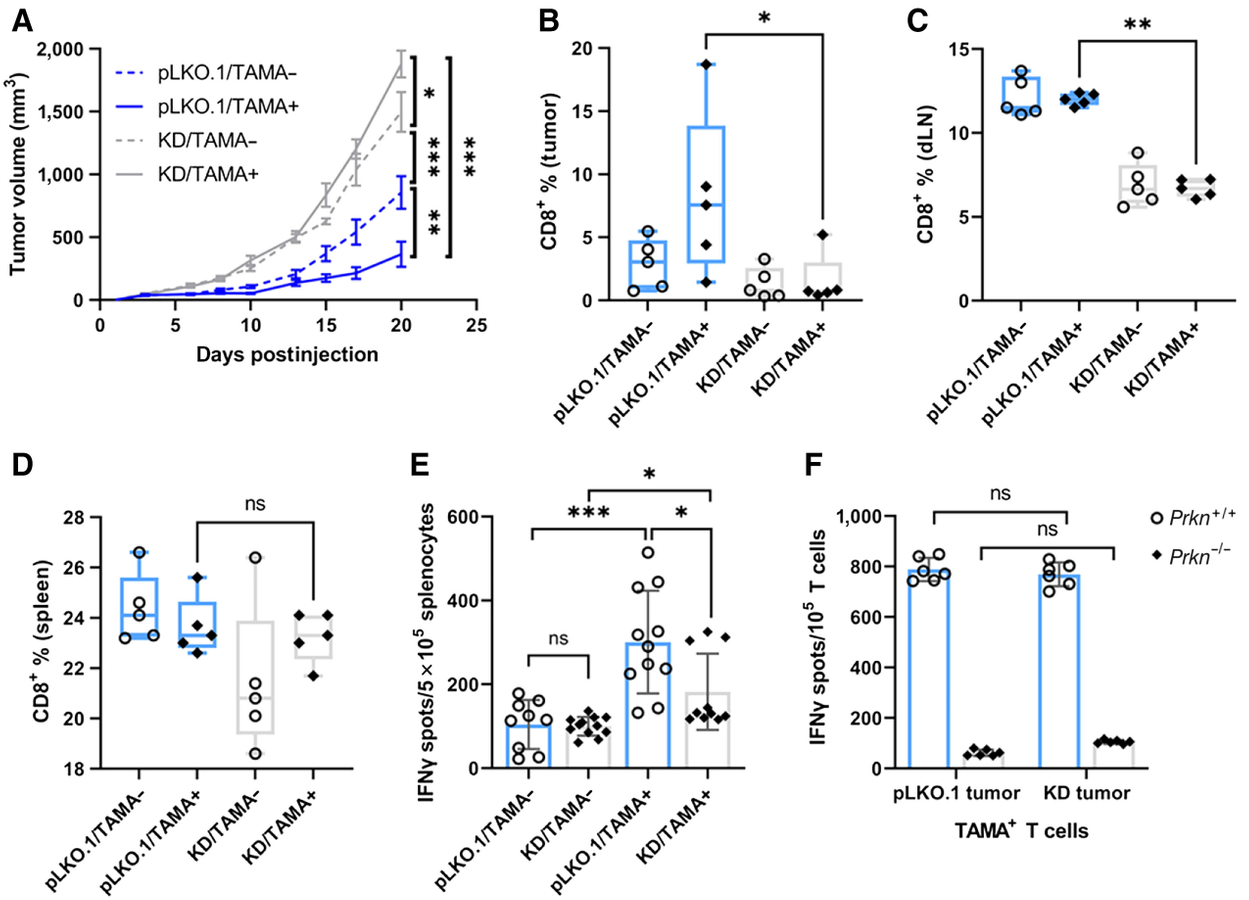

Figure 2.

Lack of Parkin undermines the effectiveness of a TAMA DC immunization. **A,** BALB/c mice (>7 per group) were challenged subcutaneously with 10^6 RENCA cells (Parkin KD or pLKO.1) in the back. At days 3, 10, and 17, the TAMA+ groups received 5×10^5 bone marrow–derived DCs pulsed with mitochondria extracts in 100 μL of PBS, intradermally (TAMA vaccine). **B–D**, Percentage of $CD8^+$ T-cell populations found in tumor, draining lymph node (dLN), and spleen of KD or pLKO.1 tumor-challenged mice, treated (or not) with the TAMA vaccine. **E,** Splenocytes isolated from immunized mice (TAMA+) or controls (TAMA−) were restimulated overnight *in vitro* with a cocktail of COX1 ($n = 3$) and ND5 ($n = 3$) peptides (100 ng/well). T-cell reactivity was measured by IFNγ ELISPOT. **F,** Infiltrating T cells from TAMA-vaccinated mice were magnetically isolated from KD or pLKO.1 tumors. Then, cocultured overnight with stimulator Parkin-positive or -negative RENCA cells (10:1 ratio). IFNγ ELISPOT was performed to analyze T-cell activation. Data are represented as mean ± SEM. *, $P < 0.05$; **, $P < 0.01$; ***, $P < 0.001$; two-way ANOVA (**A**), and unpaired, two-tailed *t* test (**B–F**).

vaccinated counterpart. Both unvaccinated controls showed no differences following stimulation (**Fig. 2E**). In addition, we assessed the functional capacity of antigen-specific immune responses. T cells were magnetically collected from spleens of TAMA-immunized mice bearing pLKO.1 or KD tumors, and cocultured with pLKO.1 or KD antigen presenting RENCA cells. Consequently, we found that the Parkin KD cells had significantly reduced capability to activate $CD8^+$ T cells (from pLKO.1 or KD groups, indistinctively) as assessed by IFNγ ELISpot (**Fig. 2F**). Altogether, the lack of Parkin in RENCA tumors negatively impacts the efficacy of a DC-based immunotherapy by reducing $CD8^+$ T-cell tumor infiltration and TAMA recognition.

Parkin regulates cytosolic tumor antigen processing and presentation and facilitates effector $CD8^+$ T-cell cancer immunity

Our previous studies using the RENCA model showed that Parkin facilitates tumor evasion by impairing mitochondria-derived antigen presentation. To investigate whether Parkin also affects cytosol-derived antigen presentation, we generated B16(F10) melanoma cells expressing chicken ovalbumin (OVA) in the cytoplasm as a target antigen. We then knocked out Parkin using CRISPr/Cas9 (B16-OVA KO) or transduced the empty vector (EV) as a control (B16-OVA EV). Notably, the B16 tumor model has deficiencies in the expression of MHC-I APM (15). Thus, we stimulated the cells overnight with IFNγ (10 ng/mL) to assess the regulatory role of Parkin on antigen processing and presentation under ectopic upregulation of MHC-I expression. Although we found no differences at basal levels, mRNA (**Fig. 3A**) and protein (**Fig. 3B**) expression of the APM in IFNγ-stimulated B16-OVA cells were negatively impacted when Parkin was absent. As expected, B16-OVA KO cells showed a significantly reduced capability to present the H-2K(b) binding OVA (257–264)-peptide (SIINFEKL) to magnetically isolated OT.1 $CD8^+$ T cells, either in the presence or absence of IFNγ stimulation as compared with EV controls (**Fig. 3C**). Altogether, the MHC-I APM and T-cell activation were significantly downregulated in KO cells, but not abrogated, suggesting that Parkin is a key contributor in this process.

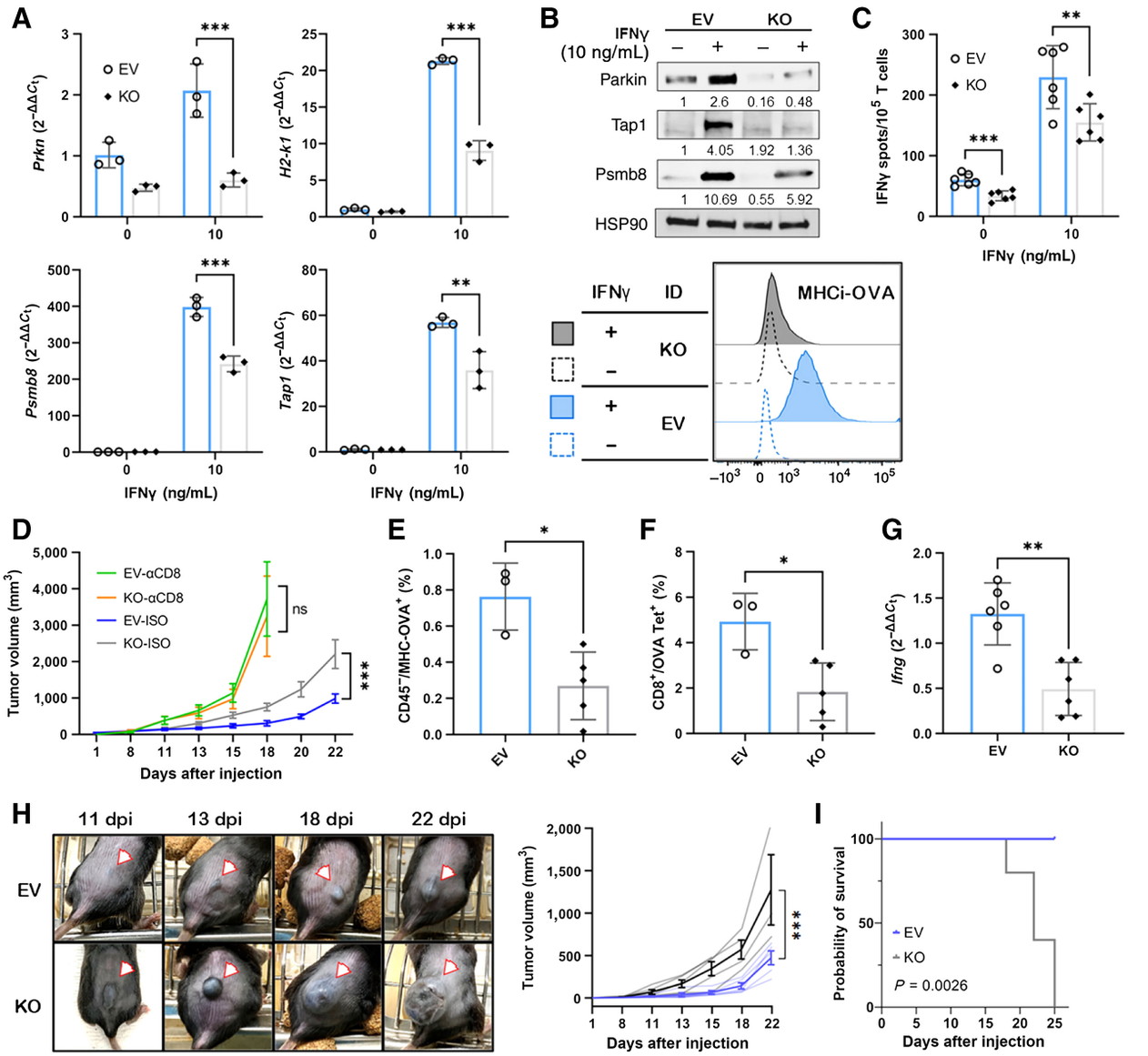

Figure 3.

Parkin regulates cytosolic tumor antigen processing and presentation and facilitates effector CD8$^+$ T-cell cancer immunity. **A–C,** Mouse melanoma B16-OVA *Prkn* knockout (KO, CRISPr/Cas9) or EV control cells were stimulated for 18 hours with IFNγ (10 ng/mL) or mock-stimulated before the analyses. **A,** mRNA expression levels of *Prkn*, *H2-k1*, *Psmb8*, and *Tap1* in B16-OVA Parkin KO or EV cells. Data are represented as mean ± SD. ** $P < 0.01$; *** $P < 0.001$; unpaired, two-tailed *t* test. **B,** Protein expression analyses of Parkin, Tap1, and Psmb8 (immunoblotting) and SIINFEKL-bound to H-2Kb (MHCi-OVA; intracellular staining, flow cytometry) of B16-OVA KO and EV cells. Data represent two to three independent experiments. **C,** IFNγ ELISPOT analysis was performed on OT.1 T cells (10^5) cocultured overnight with B16-OVA KO and EV cells in a 5:1 ratio. **D,** B16-OVA Parkin KO or EV cells (10^6) were injected in the back of C57BL/6 mice and tumor growth was monitored. Five mice per group were treated with anti-CD8 blocking antibody (aCD8) or isotype (ISO) control. **E,** Percentage of CD45$^-$/MHC-OVA$^+$ cells present in B16-OVA Parkin KO or EV isotype-treated tumors analyzed by flow cytometry. **F,** SIINFEKL-specific CD8$^+$ T-cell tumor infiltration present in B16-OVA Parkin KO or EV isotype-treated tumors. **G,** mRNA expression levels of IFNγ in B16-OVA Parkin KO or EV isotype-treated tumors. **E–G,** Data are represented as mean ± SEM. ns, not significant; *, $P < 0.05$; **, $P < 0.01$; unpaired, two-tailed *t* test. **H,** B16-OVA Parkin KO or EV cells (10^6) were injected in the back of C57BL/6-Tg (TcraTcrb)1100Mjb/J (OT.1) mice (5 per group) and tumor growth was monitored. **I,** Survival rate analysis (Kaplan–Meier, log-rank test) was performed by day 25 posttumor challenge, including five mice per group. **D** and **H,** Data are represented as mean ± SEM. ***, $P < 0.001$; two-way ANOVA.

To investigate the biological relevance of Parkin regulation of APM in the B16 murine melanoma model, we injected 1×10^6 B16-OVA KO cells or EV controls subcutaneously and tumor challenged C57BL/6 mice over 21 days. Consequently, B16-OVA tumors lacking Parkin (KO-ISO) progressed faster and larger than controls (EV-ISO; **Fig. 3D**), confirming our previous data using RENCA cells. The *in vitro* cellular proliferation of both EV and KO B16-OVA cells was similar, as assessed by clonogenic growth

(Supplementary Fig. S3A). Taken together, these data suggest that Parkin regulates cytosolic-derived antigen presentation through gene and protein modulation of the APM, which results in poor effector $CD8^+$ T-cell responses.

The presence of tumor-infiltrating lymphocytes (TIL) within adult tumors is associated with improved clinical outcomes (16). To investigate whether the lack of Parkin affects the infiltration of effector $CD8^+$ T cells into the tumor, we challenged C57L/6 mice with 1×10^6 B16-OVA KO cells or EV controls subcutaneously and treated them with depleting anti-CD8 or isotype control. The depleting antibody intraperitoneal injections were performed 2 days prior to tumor injection, on the day of tumor injection, and then twice weekly until euthanasia. As previously shown, Parkin-deficient tumors grew faster than EV controls. Interestingly, upon CD8 depletion both KO and EV tumors presented a similar trend in tumor progression, with each growing significantly faster than their respective controls (**Fig. 3D**). We performed a similar study to validate these results using the Parkin-deficient RENCA cells. Likewise, CD8 depletion resulted in faster tumor progression of both KD and pLKO.1 RENCA tumors, confirming the pivotal role of CD8 T cells in controlling cancer progression in these models (Supplementary Fig. S4). As expected, flow cytometric analysis of KO tumors revealed a significantly reduced number of cells expressing the MHC-OVA complex (**Fig. 3E**; Supplementary Fig. S3B). Tumor-infiltrating cell populations in isotype-treated mice also showed reduced OVA-specific $CD8^+$ T cells in KO tumors, suggesting that the lack of Parkin limited specific antitumor immune recognition (**Fig. 3F**; Supplementary Fig. S3C). This was associated with reduced IFNγ (**Fig. 3G**), IFNβ, Foxp3, and IL12, but similar granzyme B gene expression in KO tumors (Supplementary Fig. S3D). These findings confirm that the antitumor $CD8^+$ T cell response is mostly responsible for the control of tumor growth in this model and suggest that the lack of Parkin impedes effective tumor T-cell infiltration due to less interaction between tumor and immune cells. To evaluate the role of Parkin in the context of tumor evasion, we challenged OT.1 mice with 1×10^6 B16-OVA KO or EV cells. Interestingly, the injection of Parkin-deficient cells resulted in rapid tumor growth and lower survival rates (**Fig. 3H**). Indeed, all the mice from this group either died naturally or were sacrificed by day 25 after injection upon reaching a tumor volume of over 2,000 mm^3, versus none in the Parkin positive control group (**Fig. 3I**). These data confirm that Parkin-deficient cells have a significant advantage in evading strong and early CD8 T-cell pressure. Altogether, the lack of Parkin negatively impacts cytosolic antigen presentation in tumors by impairing the APM and reducing the infiltration of tumor-specific $CD8^+$ T cells, which in turn results in tumor evasion.

Parkin deficiency in human ccRCC is associated with poor clinical outcome, limited antigen presentation capabilities, and impacts immunotherapy efficacy

Parkin defects including loss of function mutations, diminished expression, and loss have been identified in several solid tumors including renal cell carcinoma (ccRCC; ref. 17). Indeed, after a TCGA database analysis comparing tumor vs. healthy controls, we found that Parkin gene expression is significantly downregulated in patient tumor samples and associated with overall survival (**Fig. 4A** and **B**). Interestingly, during earlier stages of this malignancy (stages II-III), we find a loss of Parkin expression associated with limited survival, which becomes significant in the most advanced form of the disease (stage IV; **Fig. 4C**). These findings suggest that the reduction in Parkin expression is associated with poor prognosis and could be potentially used as a tumor biomarker associated with poor prognosis. Additionally, to evaluate the possible impact of Parkin expression on immunotherapy in human ccRCC, immunotherapy treated patients from TCGA were divided into two groups according to *PRKN* expression: low *PRKN* expression (below 1st quartile) and high *PRKN* expression (above 3rd quartile). Although after filtration few samples were left, survival analysis using Kaplan–Meier demonstrated significant increased benefit in patients expressing *PRKN* in comparison with low *PRKN* expresser (Supplementary Fig. S5).

Next, we asked whether the regulation of APM through Parkin also occurs in human RCC cells. First, we investigated the differential gene expression of Parkin in three individual metastatic ccRCC cell lines (786-O, CAKI-I and A498) relative to HEK293 (**Fig. 4D**) and found significant downregulation. For further human APM studies, we selected the A498 cell as it expresses the HLA-A*02 serotype and the antigen NY-ESO-1 (18). Parkin was knocked out using CRISPr/Cas editing, confirmed by loss of gene and protein expression using qPCR and immunoblotting, respectively (**Fig. 4E**). Moreover, we tested the protein expression levels of the APM upon IFNγ [10 ng/mL] stimulation and found that Parkin-deficient cells were not able to recover the expression of HLA or TAP1 (**Fig. 4F**). We evaluated the capability of the A498 Parkin-deficient cells to activate donor-derived anti NY-ESO-1 T cells in a coculture setting. Consequently, Parkin KO cells prestimulated with IFNγ showed significantly worse antigen presentation compared to EV controls (**Fig. 4G**). Altogether, lower expression of Parkin in human ccRCC is associated with poor outcome and the *in vitro* loss of Parkin facilitates tumor evasion, reducing antigen presentation and consequently, antitumor-specific T cell activation.

RNA sequencing analysis identifies PI3K/Akt involvement in Parkin-dependent APM defects

To better understand the mechanism behind this phenotype, we carried out RNA sequencing profiling of genome-wide expression in Parkin KD RENCA tumors and pLKO.1 controls. The summary gene expression data are available as a supplemental file (Supplementary Table S1). We identified a total of 319 differentially expressed genes, with 138 upregulated and 181 downregulated genes from which we developed a heatmap showing expressions of statistically significant genes on the comparison between groups (**Fig. 5A**). The KEGG enrichment scatter plot analysis (https://www.genome.jp/kegg/) revealed that the differentially expressed genes were related to biological behaviors such as thermogenesis, oxidative phosphorylation and Parkinson disease, among others (**Fig. 5B**). Furthermore, the KEGG enrichment histogram showed that the most significantly altered pathways of differentially expressed genes included cytokine–cytokine receptor interaction, PI3K/Akt pathway, chemokine signaling pathway, focal adhesion, ECM receptor interaction, and protein digestion and absorption (**Fig. 5C**). We pursued the investigation of the PI3K/Akt signaling cascade because it is among the most frequently dysregulated pathways in human cancers, and its molecular components have been involved in MHC-I expression and antigen presentation, key factors that affect the susceptibility of tumors to immunosurveillance (8, 9, 19, 20).

To validate our ccRCC human and mouse models with the previously described regulatory role of Parkin, we tested basal expression levels of individual PTEN/PI3K/Akt pathway components. As expected, we found that Parkin-deficient cells (either human A498 KO or mouse RENCA KD) demonstrated impaired mitochondrial ATP production and increased levels of iNOS activity (**Fig. 5D** and **E**).

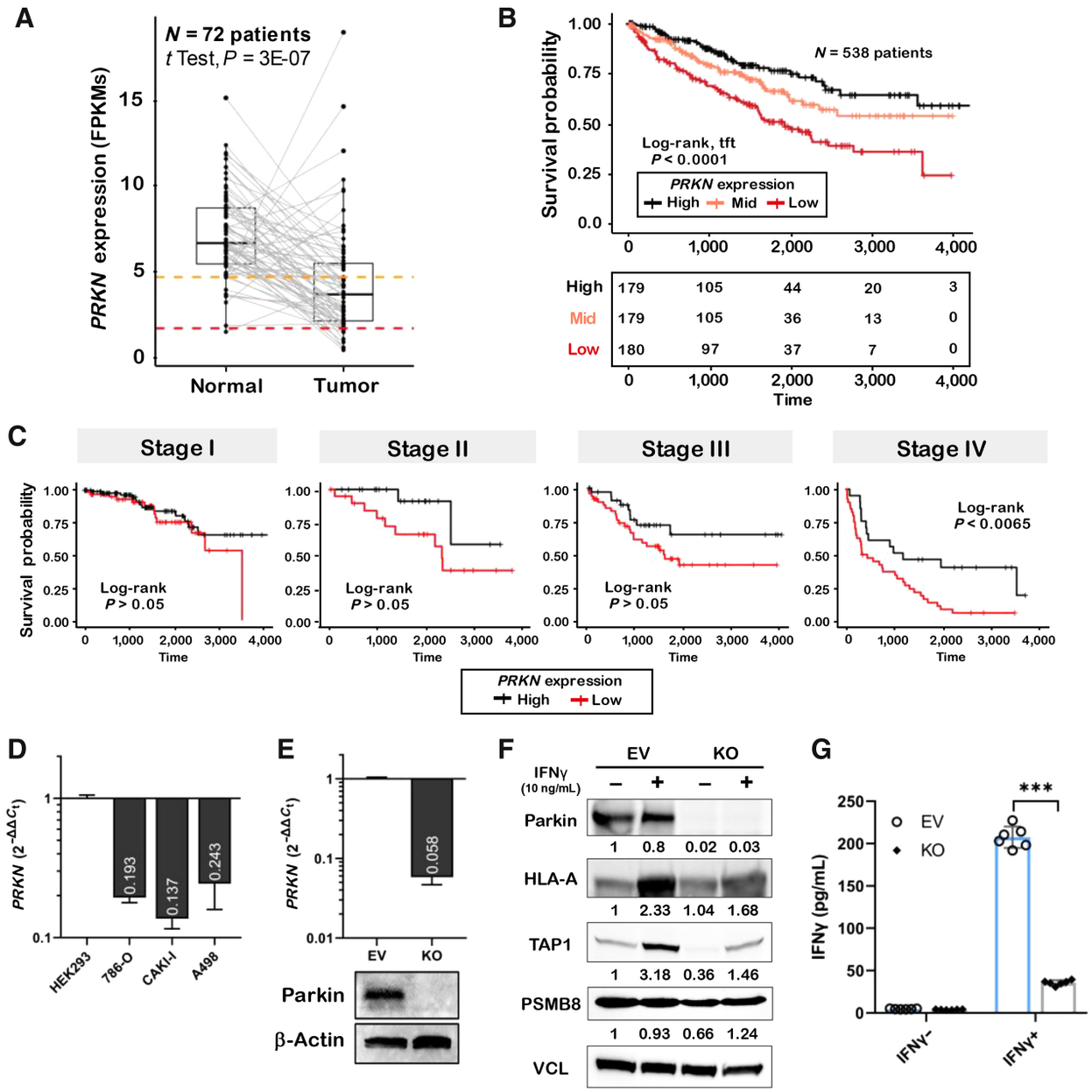

Figure 4.

Parkin deficiency in human ccRCC is associated with poor clinical outcome, limited antigen presentation capabilities, and impacts immunotherapy efficacy. Parkin (*PRKN*) downregulation in patients with KIRC is significantly associated with overall survival and tumor stage. **A,** *PRKN* gene expression is significantly downregulated in patient tumor samples vs. matched controls ($N = 72$ matches samples, P value $= 3E{-}07$ via paired Student t test; FPKMs mapped reads data from GDC HTSeq-FPKM pipeline was used). Dashed lines represent cutoffs used to bin patients with KIRC into low, mid, high *PRKN* gene expression levels. **B,** *PRKN* gene expression levels are significantly associated with overall survival ($N = 538$ tumor samples, $P < 0.0001$ via log-rank test for trend). **C,** *PRKN* expression is significantly associated with overall survival in patients with stage 4 tumors (log-rank $P < 0.007$). **D,** mRNA expression levels of *PRKN* on HEK293, 786-O, CAKI-I, and A498 cells cultured overnight in growth media. **E,** mRNA and protein expression levels of A498 Parkin KO or EV cells. **F,** A498 Parkin KO or EV cells were stimulated with IFNγ (10 ng/mL) for 18 hours. Then, immunoblotting analysis was performed on Parkin, HLA-A, TAP1, and PSMB8. Data represent two to three independent experiments. Immunoblot data represent two to three independent experiments. **G,** IFNγ ELISA analysis was performed on donor-derived NY-ESO-1-specific T cells (5×10^4) cocultured in a 1:1 ratio overnight with A498 Parkin KO or EV cells. Tumor cells were prestimulated with IFNγ (10 ng/mL) or mock-treated for 18 hours before the assay. Data are represented as mean ± SD. ***, $P < 0.001$; unpaired, two-tailed t test.

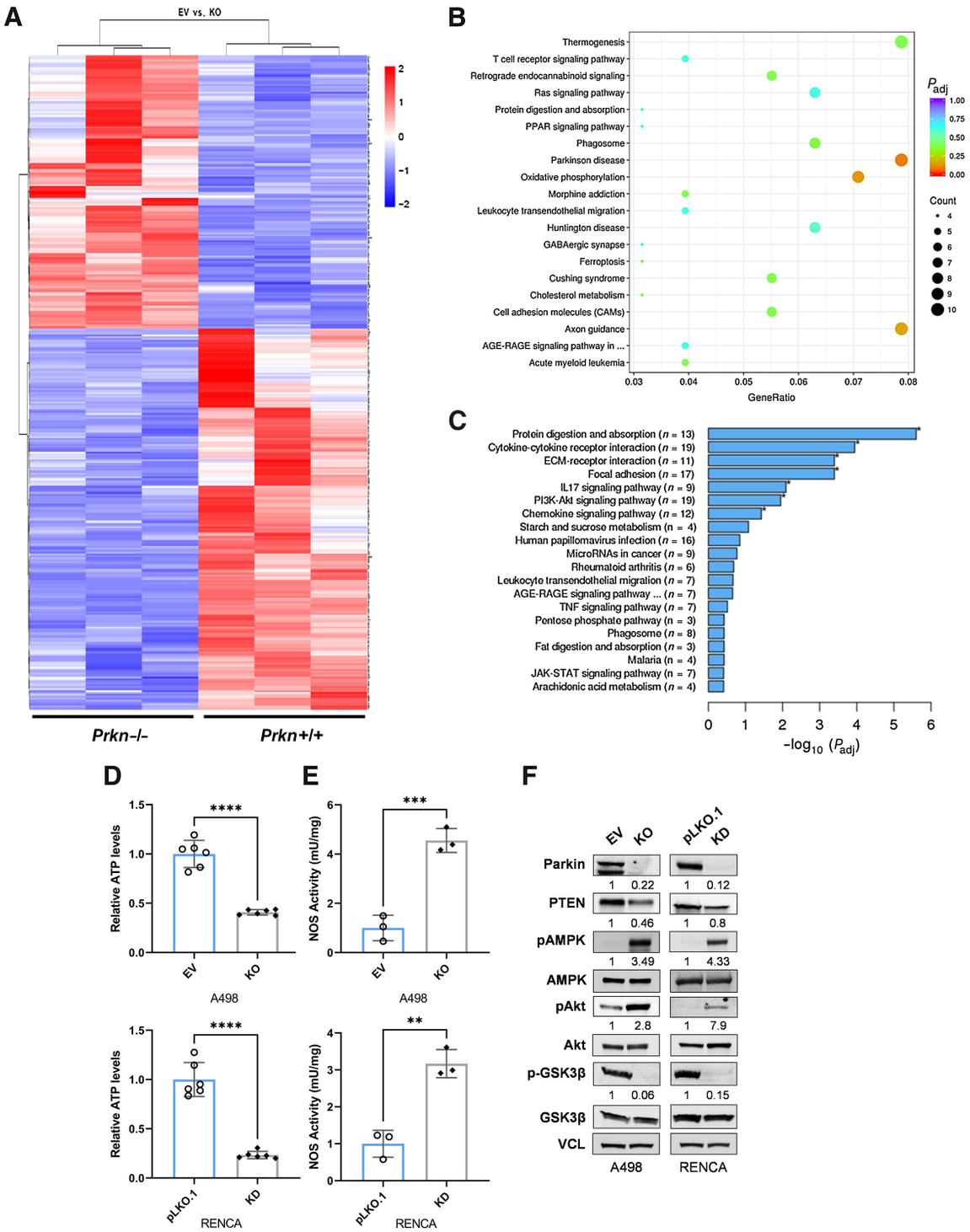

Figure 5.

RNA sequencing analysis identifies PI3K/Akt involvement in Parkin-dependent APM defects. **A,** Heatmap shows expressions of statistically significant genes on the comparison between Parkin EV and Parkin KO. **B** and **C**, KEGG enrichment scatter plot and KEGG enrichment histogram analysis, respectively. **D–F**, A498 Parkin KO or EV, and RENCA Parkin pLKO.1 or KD were cultured for 18 hours in growth media supplemented with 1% FBS. Then, relative ATP levels (**D**) and nitric oxide synthase (NOS) activity (**E**) were measured following the manufacturer's indications. **F,** Immunoblotting analysis of Parkin, PTEN, pAMPK, AMPK, pAkt, Akt, p-GSK3β, and GSK3β on A498 Parkin KO or EV, and RENCA Parkin pLKO.1 or KD cells. Data represent two to three independent experiments. Data are represented as mean ± SD. **, $P < 0.01$; *** $P < 0.001$; ****, $P < 0.0001$; unpaired, two-tailed t test.

This finding is associated with AMPK overactivation, resulting in PTEN reduction. Consequently, as PTEN is the natural inhibitor of the PI3K/Akt pathway, we also observed heightened Akt activation and enhanced dephosphorylation of downstream molecules such as GSK3β in Parkin-deficient cells (**Fig. 5F**; ref. 21). Collectively, the loss of Parkin in both mouse and human RCC results in mitochondrial metabolic defects that trigger Akt activation through the dysregulation of AMPK and PTEN.

Parkin regulates antigen presentation through the Akt signaling network

To validate the association of Parkin with Akt activation status and APM capabilities, we knocked-in (KI) Parkin into the KO cells by silencing the CRISPR/Cas system. Interestingly, the KI cells reestablished phospho-Akt and HLA-A expression to control levels (**Fig. 6A**). Subsequently, when cocultured with NY-ESO-specific T cells to assess for T-cell activation, their antigen presentation capabilities were restored (**Fig. 6B**). These findings substantiate the notion that Parkin impacts antigen presentation through the regulation of Akt activation.

Because the lack of Parkin results in over activation of Akt in tumors, we asked whether pharmacologic inhibition of Akt would overcome the loss of APM capabilities. We selected the small molecule MK2206-2HCl, a specific inhibitor of the Akt 1/2/3 isoforms evaluated in a phase II clinical trial for breast cancer (22). After testing for cell viability following increasing MK2206-2HCl concentrations over 24 hours, we chose a 10 μmol/L dose for subsequent experiments (**Fig. 6C**). We found that HLA-A protein expression increases in Parkin-deficient cells upon treatment with MK2206-2HCl (**Fig. 6D**). This was associated with a modest but significant increase in T-cell activation capabilities of A498 KO cells (**Fig. 6E**). Our data suggest that inhibition of Akt alone does not induce antigen presentation capabilities. However, the combination of MK2206-2HCl with IFNγ, enhances T-cell activation in Parkin-deficient cells.

Inhibition of Akt *in vivo* rescues TAMA immunotherapy efficacy

To investigate whether treatment with MK2206-2HCl *in vivo* could rescue the potency of the TAMA vaccine, we challenged Balb/c mice with Parkin-deficient (KD) RENCA cells. This model represents an advanced stage of tumor development where the expression levels of

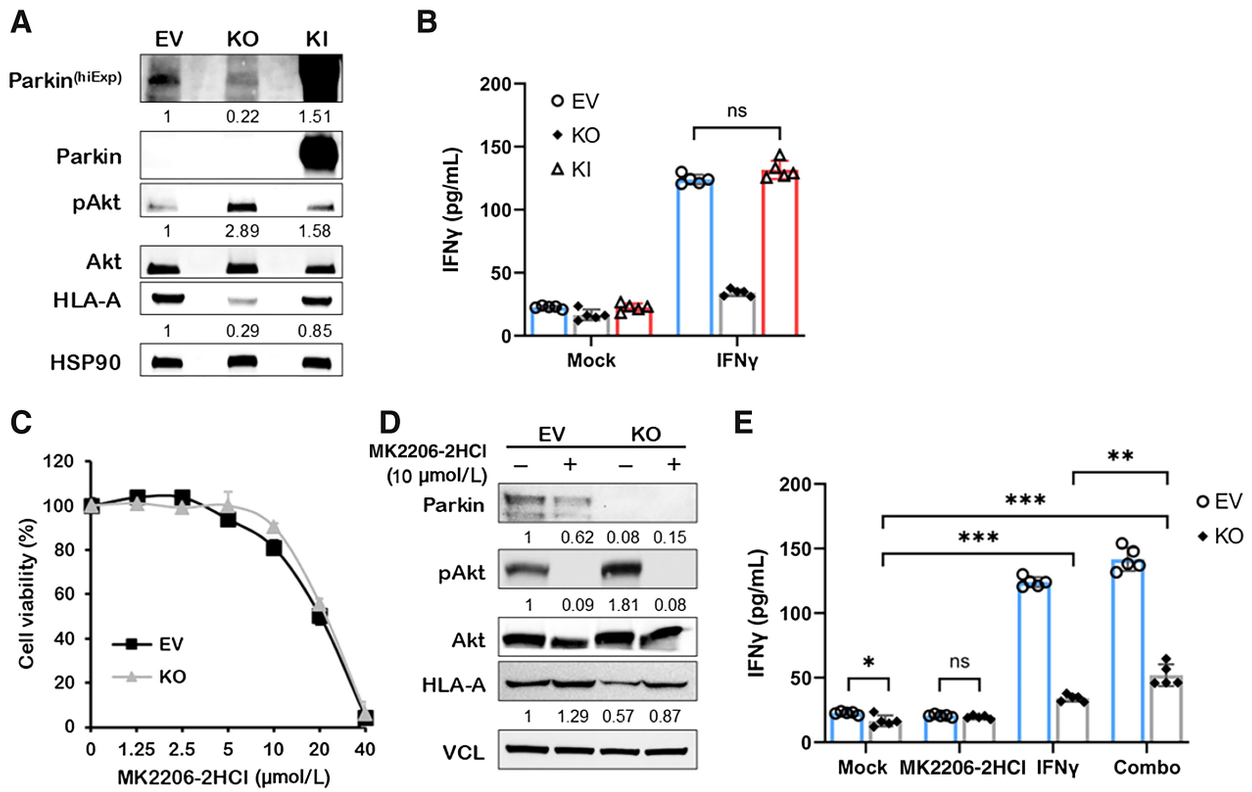

Figure 6.

Parkin regulates antigen presentation through the Akt signaling network. **A,** Immunoblotting analysis of Parkin, pAkt, Akt, and HLA-A of A498 Parkin EV, KO or knock-in (KI) cells. hiExp, high exposure. **B,** IFNγ ELISA analysis was performed on donor-derived NY-ESO-1–specific T cells (5×10^4) cocultured in a 1:1 ratio overnight with A498 Parkin EV, KO, or KI cells. Tumor cells were prestimulated with IFNγ (10 ng/mL) or mock-treated for 18 hours before the assay. Data are represented as mean ± SD. ns, not significant; unpaired, two-tailed *t* test. **C,** Drug–dose response curves of A498 Parkin EV or KO cells treated with increasing concentrations of MK2206–2HCl for 24 hours. **D,** A498 Parkin KO or EV cells were treated with MK2206–2HCl (10 μmol/L) for 18 hours. Then, immunoblotting analysis of Parkin, pAkt, Akt, and HLA-A was performed. **E,** IFNγ ELISA analysis was performed on donor-derived NY-ESO-1–specific T cells (5×10^4) cocultured in a 1:1 ratio overnight with A498 Parkin KO or EV cells. Tumor cells were prestimulated with IFNγ (10 ng/mL), MK2206–2HCl (10 μmol/L), the combination of both (Combo), or mock-treated for 18 hours before the assay. **A** and **D**, Immunoblot data represent two to three independent experiments. Data are represented as mean ± SD. **, $P < 0.01$; ***, $P < 0.001$; unpaired, two-tailed *t* test.

Parkin have dramatically decreased and hence, tumor evasion capabilities are enhanced. As described previously (23), we administered MK2206-2HCl (120 mg/kg per mouse) orally three times per week alone or in combination with the TAMA vaccine. These groups were compared against TAMA-only or mock controls. As shown earlier, the TAMA vaccine did not have a strong antitumor effect and these results were comparable with the use of inhibitor alone. Importantly, we found an additive effect when both treatments were combined, resulting in a significant control over tumor growth (**Fig. 7A**). Although this approach did not result in full tumor rejection, we were capable of significantly delaying the growth of a tumor that hides from the immune system. Furthermore, we confirmed that the T cells from both TAMA-vaccinated groups were reactive against the mitochondrial antigens by stimulating splenocytes from each mouse group with the cocktail of COX1 and ND5 peptides (**Fig. 7B**). Interestingly, we found an increased population of $CD45^+CD3^+$ cells in the tumors of TAMA-vaccinated mice (**Fig. 7C**) and more IFNγ-producing $CD8^+$ T cells in the tumors of mice treated with the combination therapy (**Fig. 7D**). Mice treated only with MK2206-2HCl did not show an enhancement in antitumor T-cell reactivity, suggesting a major contribution of a non-Akt-dependent pathway. Next, we modeled an *in vitro* system to evaluate the activation capabilities of these T cells against RENCA tumors following the treatment with MK2206-2HCl. Here, RENCA KD cells or EV (pLKO.1) controls were prestimulated overnight with MK2206-2HCl (10 μmol/L) and IFNγ (10 ng/mL) to inhibit Akt activation and to induce antigen presentation capabilities. Then, tumor cells were cocultured with T cells isolated from the spleens of mice treated with MK2206-2HCl, TAMAs, MK2206-2HCl+TAMAs, or mock-treated in an ELISpot setting. As expected, T cells were significantly more reactive in contact with RENCA

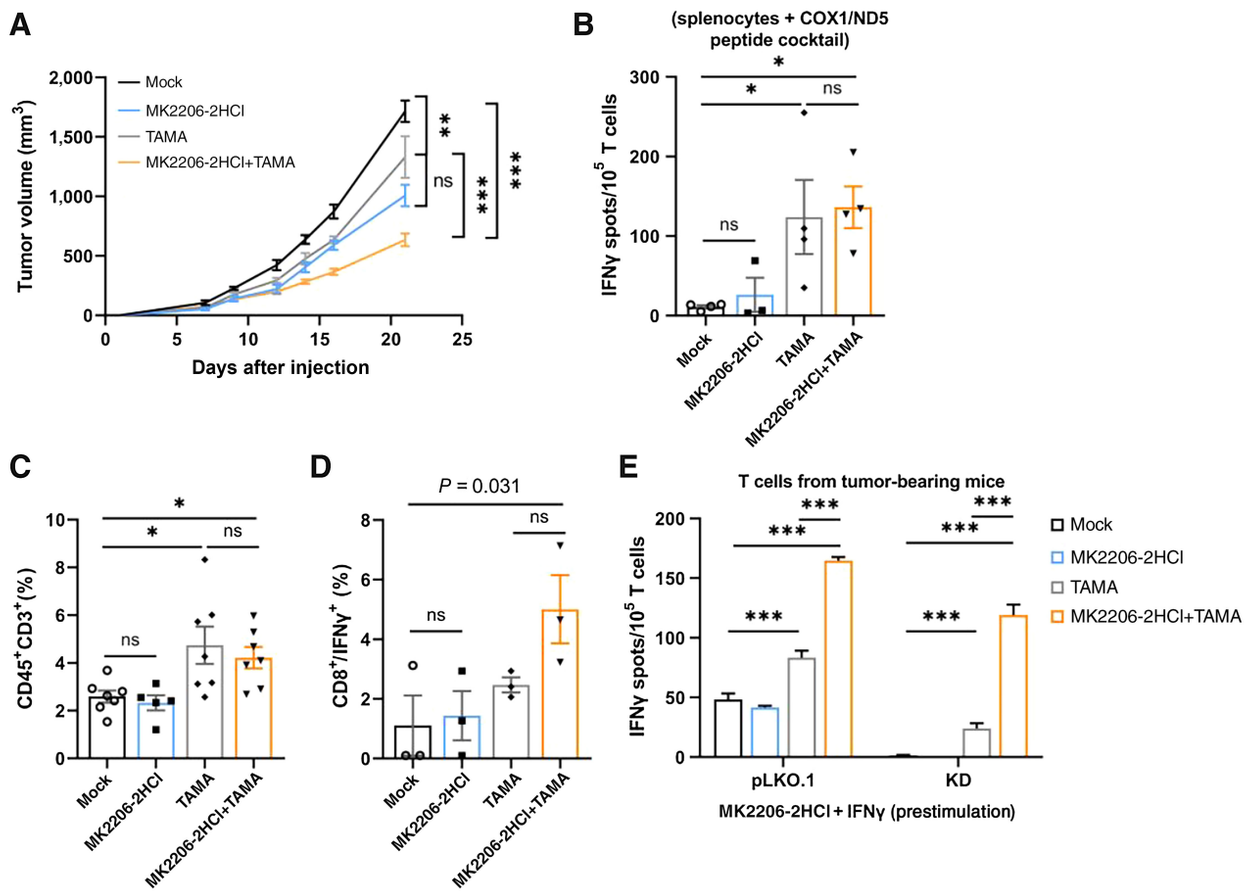

Figure 7.

Inhibition of Akt *in vivo* rescues TAMA immunotherapy efficacy. **A,** BALB/c mice (>7 per group) were challenged subcutaneously with 10^6 Parkin KD RENCA cells in the back. At days 3, 10, and 17, the TAMA+ groups received 5×10^5 bone marrow–derived DCs pulsed with mitochondria extracts in 100 μL of PBS, intradermally (TAMA vaccine). Moreover, we administered MK2206–2HCl (120 mg/kg per mouse) orally three times per week alone or in combination with the TAMA vaccine. **B,** Splenocytes isolated from each group were restimulated overnight *in vitro* with a cocktail of COX1 ($n = 3$) and ND5 ($n = 3$) peptides (100 ng/well). T-cell reactivity was measured by IFNγ ELISPOT. **C** and **D,** Percentage of infiltrating $CD45^+/CD3^+$ (**C**) and activated $CD8^+/IFN\gamma^+$ (**D**) T cells in Parkin KD tumors from each group evaluated by flow cytometry. **E,** T cells were magnetically isolated from KD tumors of each group. Then, cocultured overnight with stimulator Parkin KD or pLKO.1 RENCA cells (10:1 ratio). RENCA cells were pretreated for 18 hours with the IFNγ (10 ng/mL) and MK2206–2HCl (10 μmol/L) combination. IFNγ ELISPOT was performed to analyze T-cell activation. Data are represented as mean ± SEM. ns, not significant; *, $P < 0.05$; ** $P < 0.01$; ***, $P < 0.001$; two-way ANOVA (**A**), and unpaired, two-tailed *t* test (**B–E**).

pLKO.1 controls than with RENCA KD cells. Importantly, Parkin-deficient cells significantly improved T-cell activation when cocultured with T cells isolated from MK2206-2HCl-TAMA-treated mice or in a lesser extent, with TAMA-vaccinated mice (**Fig. 7E**). T cells from MK2206-2HCl- or mock-treated mice did not show reactivity against RENCA KD cells. Altogether, our data suggest that Akt inhibition in combination with the DC-TAMA vaccine *in vivo* overcomes tumor evasion associated to Parkin deficiency. Our approach enhances the efficacy of immunization by facilitating tumor antigen presentation, T-cell tumor infiltration, and $CD8^+$ T-cell reactivity.

Discussion

A growing body of evidence remarks the role of Parkin as a tumor suppressor involved in a number of cellular processes, including the downregulation of cell cycle and proliferation, migration, invasion and metastasis, mitophagy, and metabolic reprogramming (3, 24, 25). Indeed, epidemiologic, genetic and bioinformatics studies have shown multiple defects in the *PRKN* gene, localized in human chromosome 6q25–27, a region frequently lost in cancers (17, 26, 27). In this study, we show a novel role of Parkin in tumor immune surveillance through the dysregulation of the PTEN/PI3K/Akt pathway, involving the modulation of the APM and subsequent development of antitumor-specific $CD8^+$ T-cell reactivity. Thus, during the progression of cancer, the presence of Parkin mutations that result in loss of its functionality can facilitate the development of tumor evasion mechanisms. Furthermore, the development of new therapies/drugs or treatment protocols should evaluate Parkin expression within the tumor, as loss could impair the therapeutic effectiveness, particularly of immunotherapies.

Here, we generated murine and human models that resemble advanced-stage tumors, where Parkin deficiencies are found. In the subcutaneous xenograft mouse models, we observed an aggressive tumor growth in the absence of Parkin that was associated with poor tumor antigen presentation and antitumor $CD8^+$ T-cell infiltration and activation. These observations were consistent in a renal orthotopic model (Supplementary Figs. S1A–S1D). Thus, suggesting that tumor-intrinsic Parkin deficiencies impact antigen presentation affecting tumor immune evasion independently of the tumor site. Importantly, the DC-based TAMA immunization against mitochondria-derived antigens in RENCA KD tumors lost its efficacy, showing the crucial role of Parkin in tumor development and upon antitumor cellular therapeutic strategies. Moreover, we found that the lack of Parkin negatively impacts cytosol-derived antigen presentation and $CD8^+$ T-cell immunity as evaluated in the B16-OVA model.

Parkin has a key role in modulating inflammatory responses, especially during late stages in cancer progression when heightened genetic and protein expression defects are observed. Preclinical studies have demonstrated that inhibition of mitochondria DNA repair pathways, especially the base excision repair (BER) pathway focused on reactive oxygen species (ROS)–induced lesions, enhance tumor sensitivity when provided in combination with anticancer drugs and radiation (28). Parkin actively participates to help reduce mitochondrial genome damage by ROS and supports mitochondria DNA (mtDNA) recovery through promotion of mitophagy (29, 30). Consequently, the accumulation of damaged mitochondria found in tumors is associated with poor outcome (31). In addition, Parkin regulates immune responses by triggering innate immune system receptors via mitophagy or xenophagy (32); by interacting with MAVS (mitochondrial antiviral signaling protein), resulting in poor IRF3 activation and antiviral response (33); by activating the STING1/TMEM173-mediated DNA sensing pathway through mtDNA stress, leading to autophagy-dependent ferroptosis and STING-associated inflammation (34, 35); by controlling the mtROS–NLRP3 axis-mediated inflammation (36); or by facilitating K63 ubiquitination of RIPK1, promoting the activation of nuclear factor-κB (NF-κB) and mitogen-activated protein kinases (MAPK; ref. 37). The by-products of these signals can promote cytoplasmic dimerization of STAT1/STAT1 and STAT1/STAT2 in an autocrine and paracrine manner (38), ultimately activating NLRC5, the master regulator of the MHC-I antigen processing and presentation machinery (39). Because of its active role in mitochondria-associated metabolic stress alleviation and inflammation, we speculate that Parkin defects developed as cancer progresses can be a dynamic mechanism allowing adaptation of tumor cells. This strategy results in the reduction of their capabilities to process and present antigens in the context of MHC-I, affecting antitumor T-cell reactivity, and limiting effective immune surveillance. Further studies must be carried on to better understand the molecular mechanistic interaction between Parkin and NLRC5 in tumors, as the latter has been demonstrated to regulate the APM, $CD8^+$ T-cell activation, and tumor evasion (39).

Throughout our studies we have shown that Parkin mediates antigen presentation capabilities in cancer cells, facilitating tumor evasion when defective. Indeed, Parkin-deficient RENCA cells harboring TAMAs show an aggressive tumor growth and are not susceptible to TAMAs immunization (**Fig. 2A**). Interestingly, *in vivo* CD8 depletion assays revealed similar tumor growth dynamics between anti-CD8-treated and control KD RENCA tumors (Supplementary Fig. S4), suggesting that the lack of Parkin in this model system results in an immune evasion phenotype comparable with mice deprived of CD8 T cells. Furthermore, Parkin-deficient B16-OVA cells injected in C57BL/6 or OT.1 mice resulted in faster tumor growth and lower survival rates as compared with controls (**Fig. 3D**, **H**, and **I**). These data confirm that tumor cells lacking Parkin have a significant advantage to evade both, therapeutic immunization and a strong and early T-cell pressure, respectively. Importantly, the aggressiveness of Parkin-deficient tumor cells could also be explained by the rapid emergence of genetic variations tolerant to the potent T-cell response as discussed by Kaluza and colleagues (40). Together, while facilitating antitumor $CD8^+$ T-cell immunity, Parkin could also prevent immunoediting and the expansion of more aggressive tumor mutants capable to escape immune surveillance.

Our TCGA survival analysis revealed that patients in advanced-stage (stage IV) ccRCC present a significantly worse clinical outcome when the expression of Parkin is low. This observation was confirmed *in vitro* by evaluating the expression of Parkin using metastatic human ccRCC cell lines. Likewise the murine models, the APM and $CD8^+$ T-cell activation were significantly downregulated upon CRISPr/Cas removal of Parkin from A498 cells (**Fig. 4E–G**). Then, we investigated the differential gene expression profile of Parkin-deficient mouse tumors using RNA sequencing. Our interest in antigen presentation lead to the selection of the PI3K/Akt signaling cascade, which had been associated with the regulation of antigen presentation. Indeed, our studies confirmed the data of previous groups that showed that Parkin deficiencies are associated with mitochondria metabolic stress, AMPK activation, and PTEN degradation (**Fig. 5D–F**), ultimately resulting in Akt over activation and dysregulation of antigen presentation (7–9, 41). Importantly, A498 cells that were genetically modified to overexpress Parkin, recovered Akt activation, HLA-A expression, and antigen presentation control levels. Moreover, inhibition of Akt in Parkin KO cells could

increase antigen presentation capabilities only in combination with IFNγ stimulation, suggesting that this process is orchestrated primarily by Parkin and enhanced by the IFNγ/STAT1 axis (9, 20, 42).

Immunotherapeutic approaches have shown to benefit patients with preexisting T-cell responses against their tumor, as evidenced by a baseline $CD8^+$ T-cell infiltration within the tumor microenvironment (43, 44). However, efficient APM capabilities (and subsequent spontaneous antitumor T-cell response), T cell–mediated tumor killing, and T-cell trafficking into tumors can be negatively impacted by the loss of PTEN (45) or abnormal signaling of the cell-intrinsic oncogenic pathway, WNT/β-catenin (46). Because Parkin regulates both signaling pathways (47, 48), these suggest a direct connection between markers of cancer immune evasion and resistance to immunotherapies. Although the public clinical data in the TCGA of immunotherapy-treated KIRC patients is not abundant, our analysis suggest that those with lower Parkin expression have poor survival rates (Supplementary Fig. S5).

$CD8^+$ T cells differentiation into central memory T cells (T_{CM}) define the strength of the antitumor immunity due to their higher proliferative potential following antigen reencounter. *Abu-Eid* and colleagues have shown that inhibition of Akt1 and Akt2 enhances $CD8^+$ T-cell differentiation into the T_{CM} phenotype, delays $CD8^+$ T-cell exhaustion, and preserves naïve and T_{CM} $CD8^+$ T cells, enhancing their proliferative ability and survival (49). Furthermore, inhibition of the PI3K/Akt pathway results in selective depletion of suppressive T regulatory cells, leading to a significant therapeutic antitumor effect (50). As Parkin expression cannot be reestablished in clinical settings and Akt inhibitors promote antitumor immune responses, we evaluated the antitumor capabilities of the TAMA immunization upon Akt inhibition in Parkin-deficient tumor-bearing mice (**Fig. 7A–E**). Both Akt inhibition and TAMA vaccination as single modalities reduced tumor development. Furthermore, TAMA vaccination alone or in combination with MK2206-2HCl led to T-cell migration into the tumor. Interestingly, only the combination therapy resulted in markedly reduced tumor growth along with an increase in $CD8^+$ $IFN\gamma^+$ tumor-infiltrating T cells. Thus, despite the inherent evasive capabilities of this tumor, our approach achieved significant antitumor T-cell activity against Parkin-deficient RENCA cells.

Overall, we have described Parkin and Akt as two major biologic nodes associated with the generation of tumor immune evasion mechanisms. Parkin's newly identified ability to regulate the APM highlights the importance of its assessment when evaluating immunomodulating cancer treatments. To enhance the effectiveness of cellular- and vaccine-based cancer immune therapies in the absence of Parkin, further studies should be carried out utilizing the combination of immune checkpoint and Akt inhibitors.

Authors' Disclosures

R. Perales-Linares reports grants from NCI during the conduct of the study. M.T. Lotze reports being a member on the scientific advisory board of iRepertoire Inc. No disclosures were reported by the other authors.

Authors' Contributions

R. Perales-Linares: Conceptualization, data curation, formal analysis, supervision, validation, investigation, visualization, methodology, writing–original draft, writing–review and editing. **N. Leli:** Resources, data curation, validation, investigation, visualization, writing–review and editing. **H. Mohei:** Validation, investigation. **S. Beghi:** Investigation. **O.D. Rivera:** Data curation, software, formal analysis. **N. Kostopoulos:** Validation, investigation. **A. Giglio:** Validation, investigation. **S.S. George:** Data curation, software, investigation. **M. Uribe-Herranz:** Validation, investigation. **F. Costabile:** Validation, investigation. **S. Pierini:** Validation, investigation. **S. Pustylnikov:** Validation, investigation. **G. Skoufos:** Data curation, software, formal analysis. **Y. Barash:** Writing–review and editing. **A.G. Hatzigeorgiou:** Data curation, software, formal analysis. **C. Koumenis:** Writing–review and editing. **A. Maity:** Writing–review and editing. **M.T. Lotze:** Supervision, writing–review and editing. **A. Facciabene:** Conceptualization, resources, data curation, formal analysis, supervision, funding acquisition, project administration, writing–review and editing.

Acknowledgments

The authors would like to acknowledge Dr. Koumenis and Dr. Maity for their assistance in the logistic and departmental support. The authors thank Dr. Lotze for the assistance in the revision of the manuscript. The authors also thank Norma Carretta for her career, life advice, and financial support. The authors would like to acknowledge the funding of NIH/NCI 5R01CA206012–04 AF and NIH/NCI 1R01CA219871–01A1 AF.

The publication costs of this article were defrayed in part by the payment of publication fees. Therefore, and solely to indicate this fact, this article is hereby marked "advertisement" in accordance with 18 USC section 1734.

Note

Supplementary data for this article are available at Cancer Research Online (http://cancerres.aacrjournals.org/).

Received August 8, 2022; revised January 20, 2023; accepted August 9, 2023; published first August 14, 2023.

References

1. Beatty GL, Gladney WL. Immune escape mechanisms as a guide for cancer immunotherapy. Clin Cancer Res 2015;21:687–92.
2. Schreiber RD, Old LJ, Smyth MJ. Cancer immunoediting: integrating immunity's roles in cancer suppression and promotion. Science 2011;331:1565–70.
3. Xu L, Lin D, Yin D, Koeffler HP. An emerging role of PARK2 in cancer. J Mol Med 2014;92:31–42.
4. Cohen HT, McGovern FJ. Renal-cell carcinoma. N Engl J Med 2005;353:2477–90.
5. Levin L, Srour S, Gartner J, Kapitansky O, Qutob N, Dror S, et al. Parkin somatic mutations link melanoma and Parkinson's disease. J. Genet. Genomics 2016;43:369–79.
6. Hoxhaj G, Manning BD. The PI3K–AKT network at the interface of oncogenic signalling and cancer metabolism. Nat Rev Cancer 2020;20:74–88.
7. Numajiri N, Takasawa K, Nishiya T, Tanaka H, Ohno K, Hayakawa W, et al. On–off system for PI3-kinase–Akt signaling through S-nitrosylation of phosphatase with sequence homology to tensin (PTEN). Proc Natl Acad Sci USA 2011;108:10349–54.
8. Gupta A, Anjomani-Virmouni S, Koundouros N, Dimitriadi M, Choo-Wing R, Valle A, et al. PARK2 depletion connects energy and oxidative stress to PI3K/Akt activation via PTEN S-nitrosylation. Mol Cell 2017;65:999–1013.
9. Chandrasekaran S, Sasaki M, Scharer CD, Kissick HT, Patterson DG, Magliocca KR, et al. Phosphoinositide 3-kinase signaling can modulate MHC Class I and II expression. Mol Cancer Res 2019;17:2395–409.
10. Matheoud D, Sugiura A, Bellemare-Pelletier A, Laplante A, Rondeau C, Chemali M, et al. Parkinson's disease-related proteins PINK1 and parkin repress mitochondrial antigen presentation. Cell 2016;166:314–27.
11. Pierini S, Fang C, Rafail S, Facciponte JG, Huang J, De Sanctis F, et al. A tumor mitochondria vaccine protects against experimental renal cell carcinoma. J. Immunol 2015;195:4020–7.
12. Shalem O, Sanjana NE, Hartenian E, Shi X, Scott DA, Mikkelsen TS, et al. Genome-scale CRISPR-Cas9 knockout screening in human cells. Science 2014;343:84–87.
13. Ishihara M, Hu J, Zhang X, Choi Y, Wong A, Cano-Ruiz C, et al. Comparing metastatic clear cell renal cell carcinoma model established

in mouse kidney and on chicken chorioallantoic membrane. J Vis Exp 2020;10.3791/60314.
14. Uribe-Herranz M, Rafail S, Beghi S, Gil-de-Gómez L, Verginadis I, Bittinger K, et al. Gut microbiota modulate dendritic cell antigen presentation and radiotherapy-induced antitumor immune response. J Clin Invest 2020;130: 466–79.
15. Seliger B, Wollscheid U, Momburg F, Blankenstein T, Huber C. Characterization of the major histocompatibility complex class I deficiencies in B16 melanoma cells. Cancer Res 2001;61:1095–9.
16. Galon Jérô, Costes A, Sanchez-Cabo F, Kirilovsky A, Mlecnik B, Lagorce-Pagès C, et al. Type, density, and location of immune cells within human colorectal tumors predict clinical outcome. Science 2006;313:1960–4.
17. Toma MI, Wuttig D, Kaiser S, Herr A, Weber T, Zastrow S, et al. PARK2 and PACRG are commonly downregulated in clear-cell renal cell carcinoma and are associated with aggressive disease and poor clinical outcome. Genes Chromosomes Cancer 2013;52:265–73.
18. Adams S, Robbins F-M, Chen D, Wagage D, Holbeck SL, Morse HC, et al. HLA class I and II genotype of the NCI-60 cell lines. J Transl Med 2005;3:11.
19. Ihle NT, Abraham RT. The Pten-parkin axis: at the nexus of cancer and neurodegeneration. Mol Cell 2017;65:959–60.
20. Marijt KA, Sluijter M, Blijleven L, Tolmeijer SH, Scheeren FA, van der Burg SH, et al. Metabolic stress in cancer cells induces immune escape through a PI3K-dependent blockade of IFNγ receptor signaling. J Immunother Cancer 2019;7:152.
21. Romorini L, Garate X, Neiman G, Luzzani C, Furmento VA, Guberman AS, et al. AKT/GSK3β signaling pathway is critically involved in human pluripotent stem cell survival. Sci Rep 2016;6:35660.
22. Xing Y, Lin NU, Maurer MA, Chen H, Mahvash A, Sahin A, et al. Phase II trial of AKT inhibitor MK-2206 in patients with advanced breast cancer who have tumors with PIK3CA or AKT mutations, and/or PTEN loss/PTEN mutation. Breast Cancer Res 2019;21:78.
23. Hirai H, Sootome H, Nakatsuru Y, Miyama K, Taguchi S, Tsujioka K, et al. MK-2206, an allosteric Akt inhibitor, enhances antitumor efficacy by standard chemotherapeutic agents or molecular targeted drugs *in vitro* and *in vivo*. Mol Cancer Ther 2010;9:1956–67.
24. Devine MJ, Plun-Favreau H, Wood NW. Parkinson's disease and cancer: two wars, one front. Nat Rev Cancer 2011;11:813–23.
25. Liu J, Zhang C, Hu W, Feng Z. Parkinson's disease-associated protein Parkin: an unusual player in cancer. Cancer Commun 2018;38:40.
26. Cesari R, Martin ES, Calin GA, Pentimalli F, Bichi R, McAdams H, et al. Parkin, a gene implicated in autosomal recessive juvenile parkinsonism, is a candidate tumor suppressor gene on chromosome 6q25–q27. Proc. Natl. Acad. Sci 2003; 100:5956–61.
27. Fujiwara M, Marusawa H, Wang H-Q, Iwai A, Ikeuchi K, Imai Y, et al. Parkin as a tumor suppressor gene for hepatocellular carcinoma. Oncogene 2008;27:6002.
28. Li L-Y, Guan Y, Chen X-S, Yang J-M, Cheng Y. DNA repair pathways in cancer therapy and resistance. Front Pharmacol 2020;11:629266.
29. Rothfuss O, Fischer H, Hasegawa T, Maisel M, Leitner P, Miesel F, et al. Parkin protects mitochondrial genome integrity and supports mitochondrial DNA repair. Hum Mol Genet 2009;18:3832–50.
30. Suen D-F, Narendra DP, Tanaka A, Manfredi G, Youle RJ. Parkin overexpression selects against a deleterious mtDNA mutation in heteroplasmic cybrid cells. Proc Natl Acad Sci USA 2010;107:11835–40.
31. Brandon M, Baldi P, Wallace DC. Mitochondrial mutations in cancer. Oncogene 2006;25:4647–62.
32. Gkikas I, Palikaras K, Tavernarakis N. The role of mitophagy in innate immunity. Front Immunol 2018;9:1283.
33. Khan M, Syed GH, Kim S-J, Siddiqui A. Hepatitis B virus-induced parkin-dependent recruitment of linear ubiquitin assembly complex (LUBAC) to mitochondria and attenuation of innate immunity. PLoS Pathog 2016;12: e1005693.
34. Li C, Zhang Y, Liu J, Kang R, Klionsky DJ, Tang D. Mitochondrial DNA stress triggers autophagy-dependent ferroptotic death. Autophagy 2021;17:948–60.
35. Mao Y, Luo W, Zhang L, Wu W, Yuan L, Xu H, et al. STING-IRF3 triggers endothelial inflammation in response to free fatty acid-induced mitochondrial damage in diet-induced obesity. Arterioscler Thromb Vasc Biol 2017;37: 920–9.
36. Li J, Ma C, Long F, Yang D, Liu X, Hu Y, et al. Parkin impairs antiviral immunity by suppressing the mitochondrial reactive oxygen species-Nlrp3 axis and antiviral inflammation. iScience 2019;16:468–84.
37. Wang Y, Shan B, Liang Y, Wei H, Yuan J. Parkin regulates NF-κB by mediating site-specific ubiquitination of RIPK1. Cell Death Dis 2018;9:732.
38. Khodarev NN, Roizman B, Weichselbaum RR. Molecular pathways: interferon/stat1 pathway: role in the tumor resistance to genotoxic stress and aggressive growth. Clin Cancer Res 2012;18:3015–21.
39. Yoshihama S, Roszik J, Downs I, Meissner TB, Vijayan S, Chapuy B, et al. NLRC5/MHC class I transactivator is a target for immune evasion in cancer. Proc Natl Acad Sci USA 2016;113:5999–6004.
40. Kaluza KM, Thompson JM, Kottke TJ, Flynn Gilmer HC, Knutson DL, Vile RG. Adoptive T cell therapy promotes the emergence of genomically altered tumor escape variants. Int J Cancer 2012;131:844–54.
41. Tseng P-C, Huang W-C, Chen C-L, Sheu B-S, Shan Y-S, Tsai C-C, et al. Regulation of SHP2 by PTEN/AKT/GSK-3β signaling facilitates IFN-γ resistance in hyperproliferating gastric cancer. Immunobiology 2012;217: 926–34.
42. Sivaram N, McLaughlin PA, Han HV, Petrenko O, Jiang Y-P, Ballou LM, et al. Tumor-intrinsic PIK3CA represses tumor immunogenicity in a model of pancreatic cancer. J Clin Invest 2019;129:3264–76.
43. Harlin H, Meng Y, Peterson AC, Zha Y, Tretiakova M, Slingluff C, et al. Chemokine expression in melanoma metastases associated with CD8+ T-cell recruitment. Cancer Res 2009;69:3077–85.
44. Ji R-R, Chasalow SD, Wang L, Hamid O, Schmidt H, Cogswell J, et al. An immune-active tumor microenvironment favors clinical response to ipilimumab. Cancer Immunol Immunother 2012;61:1019–31.
45. Peng W, Chen JQ, Liu C, Malu S, Creasy C, Tetzlaff MT, et al. Loss of PTEN promotes resistance to T-cell-mediated immunotherapy. Cancer Discov 2016;6:202–16.
46. Wang B, Tian T, Kalland K-H, Ke X, Qu Y. Targeting Wnt/β-catenin signaling for cancer immunotherapy. Trends Pharmacol Sci 2018;39:648–58.
47. Rawal N, Corti O, Sacchetti P, Ardilla-Osorio H, Sehat B, Brice A, et al. Parkin protects dopaminergic neurons from excessive Wnt/β-catenin signaling. Biochem Biophys Res Commun 2009;388:473–8.
48. Yang W, Li Y, Gao R, Xiu Z, Sun T. MHC class I dysfunction of glioma stem cells escapes from CTL-mediated immune response via activation of Wnt/β-catenin signaling pathway. Oncogene 2020;39:1098–111.
49. Abu Eid R, Friedman KM, Mkrtichyan M, Walens A, King W, Janik J, et al. Akt1 and -2 inhibition diminishes terminal differentiation and enhances central memory CD8+ T-cell proliferation and survival. Oncoimmunology 2015;4:e1005448.
50. Abu-Eid R, Samara RN, Ozbun L, Abdalla MY, Berzofsky JA, Friedman KM, et al. Selective inhibition of regulatory T cells by targeting PI3K-Akt pathway. Cancer Immunol Res 2014;2:1080–9.